symmetry

MDPI

Article

Pyrroloindole-Based Dynamic Combinatorial Chemistry

Tiberiu-Marius Gianga [1,2], Dora-Maria Răsădean [1] and G. Dan Pantoș [1,*]

[1] Department of Chemistry, University of Bath, Claverton Down, Bath BA2 7AY, UK; tiberiu-marius.gianga@diamond.ac.uk (T.-M.G.); D.Rasadean@bath.ac.uk (D.-M.R.)
[2] Beamline B23, Diamond Light Source, Ltd., Chilton, Didcot OX11 0DE, UK
* Correspondence: g.d.pantos@bath.ac.uk; Tel.: +44-1225-384-376

Received: 2 April 2020; Accepted: 16 April 2020; Published: 3 May 2020

Abstract: We report a new class of building blocks for Dynamic Combinatorial Chemistry (DCC) based on the pyrroloindole scaffold. The attachment of L-cysteine on the α, α′ positions of the core makes the molecule suitable for disulfide exchange in aqueous dynamic combinatorial libraries (DCLs). The synthesis of the core follows a modified version of the Knoevenagel–Hemetsberger approach. The new building block (**L-PI**) is fluorescent (Φ = 48%) and relatively stable towards thermal and photodegradation. The chirality of the cysteine is transferred to the electron-rich pyrroloindole core. Homo- and heterochiral DCLs of **L-PI** with electron-deficient L- and D-naphthalenediimide (NDI) lead to similar library distributions regardless of the enantiomer used. When no salt is present, the major component is a dimer, while dimers and tetramers are obtained at increased ionic strength.

Keywords: dynamic combinatorial chemistry; pyrroloindoles; chirality; disulfide

1. Introduction

Dynamic combinatorial chemistry (DCC) has emerged in the last decades as a powerful tool in the development of (bio)sensors [1–3], self-replicating materials [4–7], receptors [8–11], etc. It is also a well-established approach in making interlocked molecular architectures (e.g., catenanes and knots) using simple precursors [12–31]. DCC involves reactions under thermodynamic control in which starting molecules (building blocks) combine to generate a complex mixture of species called dynamic combinatorial library (DCL) [1,32,33]. The building blocks have moieties that allow for reversible exchanges until the equilibrium is reached and the precursors are completely consumed. Representative examples [1,34] of reversible reactions include ester [35–37], imine [21,23,26], hydrazone [38,39], hydrogen-bond [40–42], acetal [43] and disulfide exchanges [15,44,45]. Among these, disulfide exchange is of particular interest as it is prevalent in biological systems (e.g., cystines) [46–48]. The reaction works close to the physiological conditions (aqueous media and pH 8), and it stops when all the thiolate anions are consumed (Scheme 1).

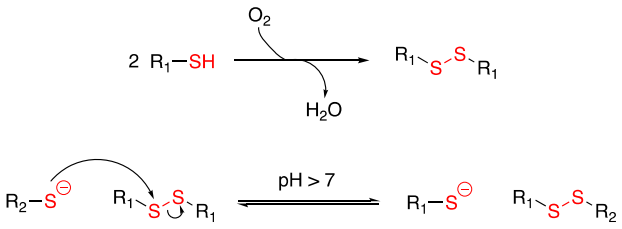

Scheme 1. General mechanism of disulfide exchange.

Disulfide exchange reactions for DCC have been largely explored by Sanders and Pantoș groups [12,13,15,16,45,49]. Their work has mainly focused on naphthalenediimide (NDI) and dialkoxynaphthalene (DN) derivatives to synthesizing interlocked molecules. Other building blocks with thiol groups allowed for the synthesis of receptors and replicators [4–6,8].

The present work expands this pool by introducing a new electron-rich building block with thiol linkages. Its behaviour as a partner for electron-deficient NDIs in DCLs is studied. The role played by chirality on the outcome of DCLs (mixtures of L and L vs. L and D enantiomers) is also explored.

2. Materials and Methods

All reagents were purchased from commercial suppliers: Acros Organics, Alfa Aesar, Fluorochem, Merck, TCI Europe and used without further purification. ^{1}H and ^{13}C NMR spectra were recorded on 500 MHz Agilent Propulse or 500 MHz Bruker Avance II+ (^{1}H NMR spectra at 500 MHz, ^{13}C NMR spectra at 125 MHz) instruments. Chemical shifts (δ) are reported in parts per million (ppm). Coupling constants are reported in Hertz (Hz), and signal multiplicity is denoted as singlet (s), doublet (d), doublet of doublets (dd), doublet of doublets of doublets (ddd), triplet (t), quartet (q), dt (doublet of triplets), td (triplet of doublets), multiplet (m) and broad (br). All spectra were acquired at 25 °C, unless otherwise stated, and were referenced to the solvent residual peaks. The common solvent impurities present in small amounts in ^{1}H and ^{13}C NMR spectra were water, acetone, CH_2Cl_2 or DMF. The microwave reactions were carried out in either CEM Discover or CEM Explorer 12 instruments. LC-MS studies were carried out on a Thermo Surveyor PDA Plus LC and LCQ classic ESI MS. LC-MS data were processed using the XCalibur software. The HRMS spectra were either acquired at the National Mass Spectrometry Facility at Swansea University. The HRMS and MS/MS spectra for the library components were done on a Bruker MaXis HD ESI-QTOF mass spectrometer for high mass accuracy, coupled to a Thermo Scientific Dionex Ultra High Performance Liquid Chromatography (UPLC) unit. Circular dichroism (CD), absorption and fluorescence data were acquired on an Applied Photophysics Chirascan spectrophotometer equipped with a Peltier temperature controller.

DCL set-up: 5 mM total concentrations (the total volume of each library was 1 mL; single component libraries contained 5×10^{-6} moles; two-component libraries contained 2.5×10^{-6} moles per component) libraries were prepared by dissolving the building blocks in 10 mM aqueous NaOH, followed by titration with 100 mM NaOH/100 mM HCl (aqueous solutions) to adjust the pH to 8. The DCL solutions were stirred in closed-capped vials for at least three days at room temperature.

LC-MS settings for ESI-MS spectra (Thermo Surveyor PDA Plus LC and LCQ classic ESI MS; negative ion) were acquired with a drying temperature of 250 °C, spray current 0.5 µA, sheath gas flow of 40 arb, spray voltage 4.5 kV, capillary voltage 13 V and tube lens −15.0 V. The mass range was set from *m*/*z* 150–2000, the number of microscans in scan time was 5, and the maximum injection time was 150.0 ms. The HPLC (High Performance Liquid Chromatography) method is reported in Supplementary Materials Section 3.

LC-MS settings for HRMS data (Bruker MaXis HD ESI-QTOF): ESI-MS spectra (negative ion) were acquired with drying temperature of 320 °C, collision energy −4 eV and dry gas 12 L/min. The mass range was set from *m*/*z* 350–3500.

MS/MS settings for HRMS data (Bruker MaXis HD ESI-QTOF)**:** parent Mass (*m*/*z*): dependant on the species, ionisation width (*m*/*z*): 20.0, collision energy: 20 eV, drying temperature 240 °C and dry gas 12 L/min.

CD and absorbance settings: experiments were performed in a 10 mm pathlength quartz cuvette, wavelength range: 250–450 nm, scan mode: 1 point/nm, time-per-point: 1 sec, bandwidth: 2 nm and temperature 23 °C. Settings for variable temperature (VT) studies: temperature range: 5–55 °C and return ramp, increment: 10 °C and setting time 45 sec.

Fluorescence settings: fluorescence spectra were collected for samples with an absorbance below 0.1 AU. Experiments were performed in a 10 mm pathlength quartz cuvette. Emission spectra: wavelength range: 250–450 nm, scan mode: 1 point/nm, time-per-point: 1 sec, excitation wavelength:

340 nm, bandwidth 8 nm, PMU: 1000 V and SEM: 2 × 4.65 nm. Excitation spectra: wavelength range: 250–400 nm, scan mode: 1 point/nm, time-per-point: 1 s, emission wavelength: 393 nm, bandwidth 6 nm, PMU: 1000 V and SEM: 1.29 × 4.65 nm.

Computational studies. Geometry optimisation was performed using Avogadro [50] (Force field: UFF, Algorithm: Conjugate gradients). This was followed by MOPAC 2016 [51] (Version 18.117 M) PM7 semiempirical optimisation using the COSMO water model with a 1 convergence factor, and Gabedit 2.5.0 [52] as interface. Q_{zz} calculations were performed with GAMESS at MP2 level.

3. Results and Discussion

3.1. Building Block Design and Properties

3.1.1. Synthesis

The pyrrolo[2,3-*f*]indole scaffold consists of a pyrrole ring condensed with the benzene ring of an indole. This is the so-called "type I pyrroloindole" found in many natural alkaloids and also widely used in medicinal chemistry research [53,54]. It is aromatic (14 π electrons) and bears cysteine appendages on the α, α' positions that confer it water solubility and ability to be involved in disulfide exchange (Figure 1).

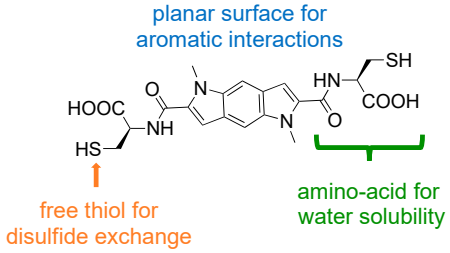

Figure 1. Structural features of the new building block designed in this work.

The initial synthesis of the core followed a previously published procedure [55]. The first step involved the formation of ethyl azidoacetate **2**, which was used in a Knoevenagel-type condensation with terephthaldehyde to yield compound **4**. The next step was the Hemetsberger reaction, giving the pyrroloindole **5**. This was obtained in low yield because most of the product polymerised—a common issue in pyrrole and pyrroloindole chemistry. Other substrates (1,4-thiophene-dialdehyde and 1,4-dimethoxy-terephthaldehyde) were used, but the Knoevenagel step worked in low yields (products **11** and **13**; further information in Supplementary Materials Section 1 and Schemes S1 and S2).

The synthetic protocol was then optimised (Scheme 2) and the Hemetsberger step carried out in more diluted conditions to prevent polymerization. Pyrrole chemistry shows that the free -NH units lead to extensive polymerization [56]. Thus, the -NH groups were alkylated, which allowed the synthesis of pure pyrroloindole **6**. The next steps included hydrolysis of the ester group to give **7**, followed by NHS activation, and *S*-trityl-L-cysteine attachment and deprotection via previously reported methods [45]. The final building block **L-PI** was obtained in 8 steps, none of which required laborious purification (experimental details in Supplementary Materials Section 1).

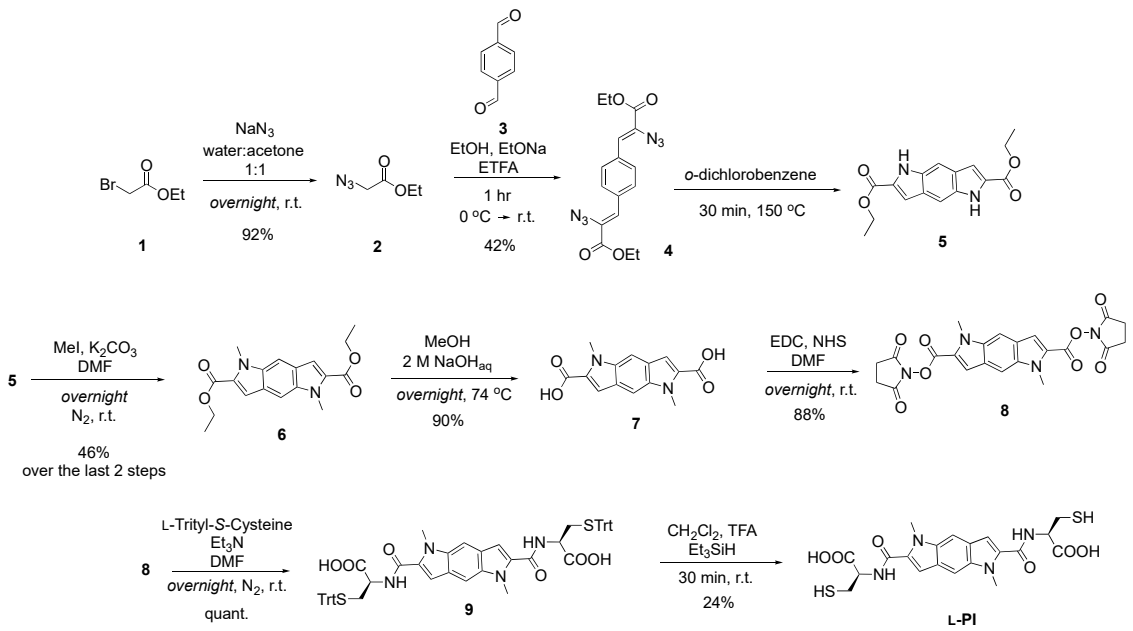

Scheme 2. Optimised protocol for the synthesis of the new building block **L-PI**. The reagents and conditions used for each step as well as the yields are indicated on the reaction arrows.

3.1.2. Optoelectronic and structural properties

The trityl-protected pyrroloindole, compound **9**, is soluble in common organic solvents, which allowed us to carry out spectroscopic studies in chloroform; the main properties are summarised in Table 1 (for molar extinction coefficient ε calculation, see Figure S14).

Table 1. Summary of the main optical properties of trityl-cysteine pyrroloindole **9** in chloroform.

Absorbance & CD			Emission	
λ_{max} (nm)	ε (L × mol^{-1} × cm^{-1})	Molar Ellipticity (deg × cm^2 × dmol^{-1})	λ_{max} (nm)	Φ (%)
327	21,600 ± 1.8	2.11×10^4	394	48

The optoelectronic and structural properties of the trityl-protected cysteine pyrroloindole **9** were assessed by UV-vis and fluorescence spectroscopy. The absorbance spectrum shows two bands centered at 280 nm and 327 nm (with a small shoulder at 345 nm), which correspond to the pyrroloindole core. The emission spectrum is characterised by a broad, intense band centered at 394 nm, with a large Stokes shift of 67 nm. The spectral features of **9** in the excitation mode are similar to those displayed by UV-vis. The quantum yield (Φ) of **9** is 48%, and has been calculated using anthracene as standard (Φ of anthracene in chloroform = 11% [57]).

The presence of the cysteine moiety allows us to explore an important feature: chirality. The pyrroloindole unit is intrinsically achiral, but the chiral information is transferred from the cysteine onto the core. We have used circular dichroism (CD) spectroscopy to analyze the chirality of the new building block precursor. The CD spectrum shown in Figure 2a displays a bisignate Cotton effect with relatively large response for a small molecule. This chirality transfer observed is not a result of aggregation as indicated by a linear Lambert–Beer plot shown in Figure S14.

The thermal stability and photodegradation of **9** over 5–55 °C temperature range and return ramp were assessed by variable temperature (VT) CD, UV-vis and fluorescence studies (Figure 2). The VT CD and UV-vis spectra show minor changes, indicating a weak temperature dependence of the chirality transfer. The CD melting profile exhibits isosbestic points, indicating a monophasic transition

across the temperature range. The VT emission and excitation spectra display irreversible thermal and photodegradation. The emission intensity drops by roughly 30%, while the excitation by almost 70%.

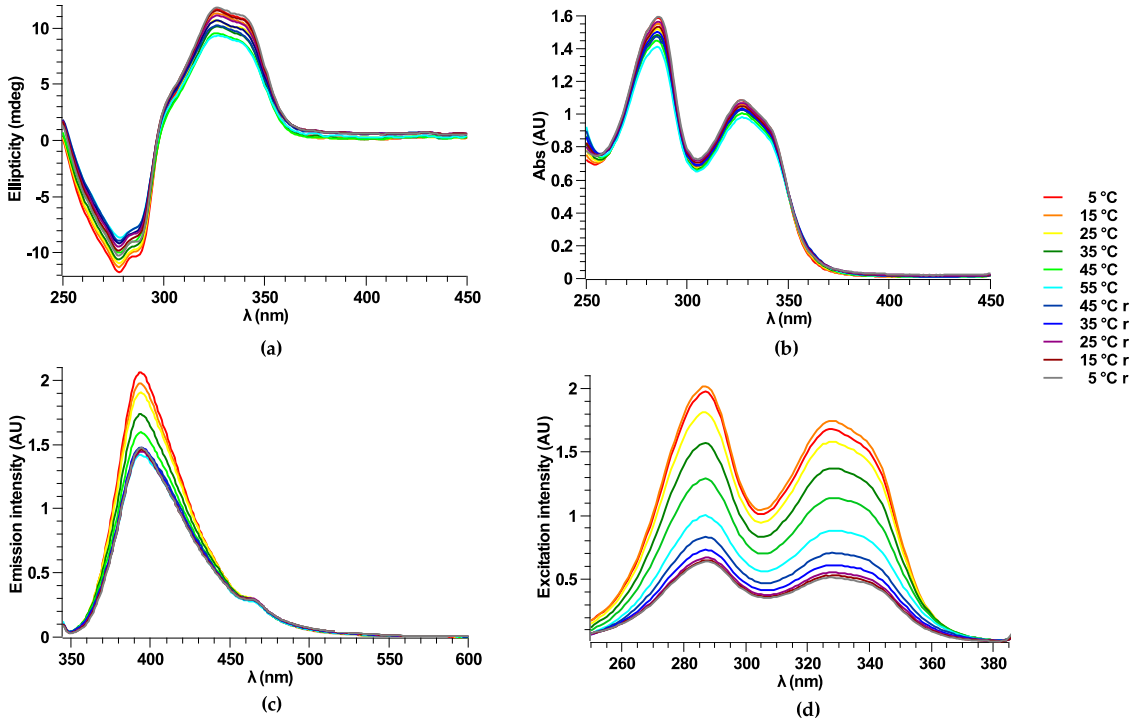

Figure 2. Thermal and photodegradation studies of **9** in chloroform at the specified temperatures (r denotes return temperature ramp) in the legend: (**a**) variable temperature (VT) circular dichroism (CD) spectra (5×10^{-5} M); (**b**) VT absorption spectra (5×10^{-5} M); (**c**) VT emission spectra (2.5×10^{-6} M); (**d**) VT excitation spectra (2.5×10^{-6} M). The sample concentration used in each experiment is given in brackets. The same color code is used for each graph.

The first indication of an electron-rich aromatic core for **L-PI** comes from its ^{1}H NMR spectrum (Figure S13), which shows peaks in the aromatic region at relatively low chemical shifts (δ 7.35 ppm). The electronic nature of organic molecules can be determined from the quadrupole moment on the z axis (Q_{zz}) calculations. The lower the number in the negative regime, the more electron-rich a molecule is. The reverse applies to electron-deficient molecules. The calculated Q_{zz} for the pyrroloindole core is −22.7 B (Buckinghams), meaning it is an electron-rich molecule. To put this number in perspective, it should be compared with the Q_{zz} of other building blocks previously used for disulfide DCC. The Q_{zz} of one of the electron-rich building blocks extensively used in DCC (2,6-DN) is −15.1 B, while the electron-deficient NDI has a Q_{zz} of 14.2 (Figure 3).

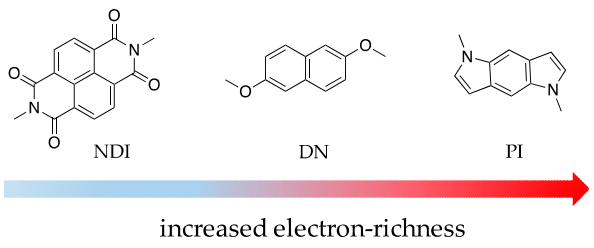

Figure 3. General structures of two main building blocks for dynamic combinatorial chemistry (DCC) and the new one designed in this work arranged in order of increased electron-richness.

3.2. Behaviour of L-PI in DCLs

3.2.1. DCLs of L-PI

One of the driving forces behind DCLs in aqueous systems is the hydrophobic effect [58]. This refers to reorganization of water molecules around a hydrophobic unit formed within the system. The hydrophobic effect is generally enhanced by adding inorganic salts [15]. Previous work in the field shows that changing either the cation (Li^+, Na^+, K^+ and Cs^+) or anion (NO_3^-, SO_4^{2-}, Br^- and Cl^-) has led to similar DCLs distribution, which is due to an increasing in medium polarity with minimum template contribution [15,45]. DCLs of **L-PI** with and without 1 M $NaNO_3$ (added to enhance the hydrophobic effect) were prepared according to the method described in Section 2. Once equilibrated, the libraries have been analyzed by HPLC, MS and MS/MS; the chromatograms are shown in Figure 4 (cartoon representations are used for clarity). The distribution of both libraries shows one major species identified as **L-PI** homodimer by MS and MS/MS analyzes (Figures S15–S17).

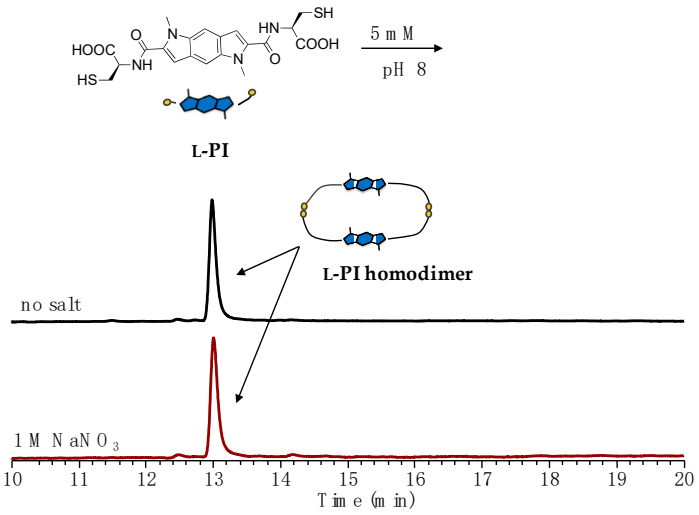

Figure 4. Reverse-phase HPLC analysis of **L-PI** (5 mM total concentration) libraries without salt (top) and in the presence of 1 M $NaNO_3$ (bottom). Absorptions recorded at 324 nm. The unlabeled peaks did not ionise and could not be identified.

3.2.2. Homochiral DCLs of L-PI and L-NDI

Another driving force behind DCLs is the donor–acceptor (D–A) interaction between electron-rich and electron-deficient aromatic cores. A representative example of an electron-deficient building block widely used in disulfide DCC is the cysteine-functionalised NDI. Homochiral libraries (i.e., same chirality of each component) of **L-PI** and **L-NDI** in 1:1 molar ratio without and with 1 M $NaNO_3$ have been prepared (Figure 5). The library with no salt contains the homochiral heterodimer (**L-PI** and **L-NDI**) as dominant species and a homochiral heterotrimer. The distribution of the DCL with 1 M $NaNO_3$ is more diverse, showing the formation of a homochiral heterotetramer at the expense of the other components. This can be due to more favorable donor–acceptor interactions between the PI and NDI cores in the structure of the tetramer while in media with high salt concentration. The sequence of tetramer (i.e., DADA or DDAA) could not be determined based on the obtained MS/MS fragmentation (Figures S26 and S27); however, this was assessed using computational studies. Complete MS and MS/MS analyses are given in Figures S18–S27.

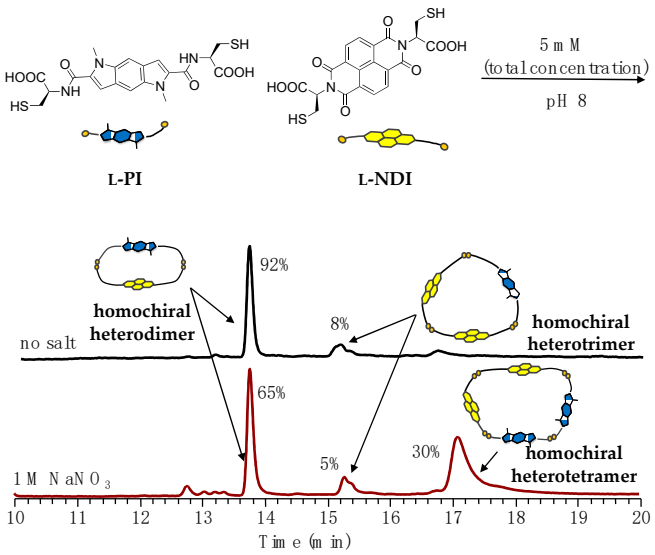

Figure 5. Reverse-phase HPLC analysis of **L-PI:L-NDI** (1:1 molar ratio, 5 mM total concentration) libraries without salt (top) and in the presence of 1 M $NaNO_3$ (bottom). Absorptions recorded at 385 nm. The unlabeled peaks did not ionise and could not be identified.

3.2.3. Heterochiral DCLs of L-PI and D-NDI

The chirality influence on the library distribution was explored by setting up heterochiral DCLs. The D enantiomer of NDI [59] was synthesised using the reported microwave-assisted method for **L-NDI** [60,61]. The **L-PI:D-NDI** mixture mainly leads to the heterochiral heterodimer when no salt is present (Figure 6). The addition of salt changes the library distribution in a similar trend to that of the homochiral DCL with $NaNO_3$: a heterochiral heterotetramer is formed (all MS and MS/MS spectra are provided in Figures S28–S32). The 1:1 molar ratio PI:NDI system does not show any chiral recognition, producing similar outcomes regardless of whether homo- or heterochiral mixture of building blocks is used. Literature reports just one example of homo- and heterochiral DCLs based on disulfide exchange, but no chiral recognition is observed either [13].

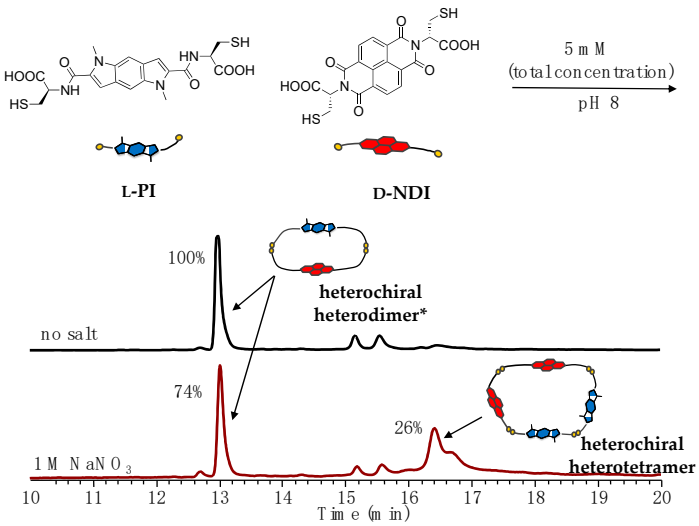

Figure 6. Reverse-phase HPLC analysis of **L-PI:D-NDI** (1:1 molar ratio, 5 mM total concentration) libraries without salt (top) and in the presence of 1 M $NaNO_3$ (bottom). Absorptions recorded at 385 nm. The unlabeled peaks did not ionise and could not be identified. * Additionally, contains **L-PI** homodimer.

The formation of macrocycles rather than interlocked molecules in pyrroloindole-based DCLs is supported by computational models. We have calculated the heat of formation of different PI-NDI cyclic oligomers (homochiral heterodimer, DDAA and DADA tetramers, and DAAD [2]catenane). These have indicated that the DDAA tetramer arrangement is the most stable among the tetrameric and catenated species.

4. Conclusions

This work reports the design and characterisation of a new building block for disulfide DCC. It is a pyrroloindole core functionalised with L-cysteine, and it respects all criteria for DCC in aqueous systems. The synthetic route is straightforward and does not require any column purification. A key step during the synthesis is the alkylation of the free -NH groups, which are prone to polymerization. The attachment of cysteine allows the chiral information to be transferred onto the otherwise achiral core, as proved by CD studies. The trityl-protected cysteine version of **L-PI** is relatively stable towards thermal and photodegradation. The new building block is also fluorescent, with a quantum yield of 48%, thus expanding its potential applications to (bio)sensing area.

Quadrupole moment calculations for the pyrroloindole core have identified it as a more electron-rich aromatic than DN (−22.7 B vs. −15.1 B). Homo- and heterochiral DCLs of **L-PI** and **L**- and **D-NDIs** have showed similar library distributions: homo- and heterodimers. The increase of ionic strength in the system by adding $NaNO_3$ has led to the formation of tetramers besides dimers.

The pyrroloindole core is versatile as α, β positions on the pyrrole ring and NH groups can be further functionalised to make new building blocks. The use of templates and other partners in DCLs can also led to different library distributions.

Supplementary Materials: The following are available online at http://www.mdpi.com/2073-8994/12/5/726/s1, Scheme S1: The reaction of **11**, Scheme S2: The reaction of **13**, Figure S1: The ^{1}H NMR spectrum of **11**, Figure S2: The ^{13}C NMR spectrum of **11**, Figure S3: The ^{1}H NMR spectrum of **13**, Figure S4: The ^{13}C NMR spectrum of **13**, Figure S5: The ^{1}H NMR spectrum of **6**, Figure S6: The ^{13}C NMR spectrum of **6**, Figure S7: The ^{1}H NMR spectrum of **7**, Figure S8: The ^{13}C NMR spectrum of **7**, Figure S9: The ^{1}H NMR spectrum of **8**, Figure S10: The ^{13}C NMR spectrum of **8**, Figure S11: The ^{1}H NMR spectrum of **9**, Figure S12: The ^{13}C NMR spectrum of **9**, Figure S13: The ^{1}H NMR spectrum of **L-PI**, Figure S14: Plot of the absorbance data versus concentration used for molar extinction coefficient (ε) calculation. The data were fitted to a linear equation, Figure S15: MS (*-ve*) of **L-PI** homodimer, Figure S16: Isotope pattern of **L-PI** homodimer (top) and its calculated isotope pattern (bottom), Figure S17: MS/MS (*-ve*) of **L-PI** homodimer, Figure S18: MS (*-ve*) of homochiral heterodimer, Figure S19: Isotope pattern of homochiral heterodimer (top) and its calculated isotope pattern (bottom), Figure S20: MS/MS (*-ve*) of homochiral heterodimer, Figure S21: MS (*-ve*) of homochiral heterotrimer, Figure S22: Isotope pattern of homochiral heterotrimer (top) and its calculated isotope pattern (bottom), Figure S23: MS/MS (*-ve*) of homochiral heterotrimer, Figure S24: MS (*-ve*) of homochiral heterotetramer, Figure S25: Isotope pattern of homochiral heterotetramer (top) and its calculated isotope pattern (bottom), Figure S26: MS/MS (*-ve*) of homochiral heterotetramer, Figure S27: Expansion of region MS/MS (*-ve*) of homochiral heterotetramer, Figure S28: MS/MS (*-ve*) of heterochiral heterodimer, Figure S29: Isotope pattern of heterochiral heterodimer (top) and its calculated isotope pattern (bottom), Figure S30: MS/MS (*-ve*) of heterochiral heterodimer, Figure S31: MS (*-ve*) of heterochiral heterotetramer, Figure S32: Isotope pattern of heterochiral heterotetramer (top) and its calculated isotope pattern (bottom), Figure S33: Simulated structure of homochiral heterodimer, Figure S34: Simulated structure of DAAD heterotetramer, Figure S35: Different views of simulated structure of DADA heterotetramer, Figure S36: Different views of simulated structure of DAAD [2]catenane, Figure S37: Plot of calculated heat of formation versus dielectric constant of different simulated structures of PI-NDI species as described in the legend. Sections: Section 1: Synthesis and characterisation of precursors and building blocks, Section 2: Characterisation of library components, Section 3: HPLC method for DCL analyses, Section 4: Computational studies of PI-NDI systems.

Author Contributions: Conceptualization, G.D.P. and T.-M.G.; writing—original draft preparation, D.-M.R. and T.-M.G.; writing—review and editing, G.D.P.; synthesis, T.-M.G.; analytical data acquisition and processing, T.-M.G. and D.-M.R.; molecular modelling: T.-M.G. and G.D.P.; supervision, G.D.P.; project administration, G.D.P.; funding acquisition, G.D.P. All authors have read and agreed to the published version of the manuscript.

Funding: This research was funded by EPSRC-DTP studentships to T.-M.G. and D.-M.R., grant numbers EB-CH1264 and EB-BB1250, respectively.

Acknowledgments: We acknowledge Shaun Reeksting from Material and Chemical Characterisation Facility at the University of Bath for MS and MS/MS analyses as well as the EPSRC UK National Mass Spectrometry

at Swansea University for high resolution mass spectrometry analyses. T.-M.G. thanks Yuto Kage for useful discussions about synthesis.

Conflicts of Interest: The authors declare no conflict of interest.

References

1. Corbett, P.T.; Leclaire, J.; Vial, L.; West, K.R.; Wietor, J.-L.; Sanders, J.K.; Otto, S. Dynamic combinatorial chemistry. *Chem. Rev.* **2006**, *106*, 3652–3711. [CrossRef]
2. Moulin, E.; Cormos, G.; Giuseppone, N. Dynamic combinatorial chemistry as a tool for the design of functional materials and devices. *Chem. Soc. Rev.* **2012**, *41*, 1031–1049. [CrossRef] [PubMed]
3. Buryak, A.; Severin, K. Dynamic combinatorial libraries of dye complexes as sensors. *Angew. Chem. Int. Ed.* **2005**, *44*, 7935–7938. [CrossRef] [PubMed]
4. Carnall, J.M.A.; Waudby, C.A.; Belenguer, A.M.; Stuart, M.C.A.; Yang, X.; Peyralans, J.J.-P.; Otto, S. Mechanosensitive self-replication driven by self-organisation. *Science* **2010**, *327*, 1502–1506. [CrossRef] [PubMed]
5. Malakoutikhah, M.; Peyralans, J.J.-P.; Colomb-Delsuc, M.; Fanlo-Virgós, H.; Stuart, M.C.A.; Otto, S. Uncovering the selection criteria for the emergence of multi-building-block replicators from dynamic combinatorial libraries. *J. Am. Chem. Soc.* **2013**, *135*, 18406–18417. [CrossRef]
6. Li, J.; Nowak, P.; Otto, S. Dynamic combinatorial libraries: From exploring molecular recognition to systems chemistry. *J. Am. Chem. Soc.* **2013**, *135*, 9222–9239. [CrossRef]
7. Sadownik, J.W.; Mattia, E.; Nowak, P.; Otto, S. Diversification of self-replicating molecules. *Nat. Chem.* **2016**, *8*, 264–269. [CrossRef]
8. James, L.I.; Beaver, J.E.; Rice, N.W.; Waters, M.L. A synthetic receptor for asymmetric dimethyl arginine. *J. Am. Chem. Soc.* **2013**, *135*, 6450–6455. [CrossRef]
9. Mullins, A.G.; Pinkin, N.K.; Hardin, J.A.; Waters, M.L. Achieving High affinity and selectivity for asymmetric Dimethylarginine by putting a lid on a box. *Angew. Chem. Int. Ed.* **2019**, *58*, 5282–5285. [CrossRef]
10. Lam, R.T.S.; Belenguer, A.; Roberts, S.L.; Naumann, C.; Jarrosson, T.; Otto, S.; Sanders, J.K.M. Amplification of acetylcholine-binding catenanes from dynamic combinatorial libraries. *Science* **2005**, *308*, 667–669. [CrossRef]
11. Bugaut, A.; Jantos, K.; Wietor, J.-L.; Rodriguez, R.; Sanders, J.K.M.; Balasubramanian, S. Exploring the differential recognition of DNA G-Quadruplex targets by small molecules using dynamic combinatorial chemistry. *Angew. Chem. Int. Ed.* **2008**, *47*, 2677–2680. [CrossRef] [PubMed]
12. Cougnon, F.B.L.; Au-Yeung, H.Y.; Pantoş, G.D.; Sanders, J.K.M. Exploring the formation pathways of donor—Acceptor catenanes in aqueous dynamic combinatorial libraries. *J. Am. Chem. Soc.* **2011**, *133*, 3198–3207. [CrossRef] [PubMed]
13. Dehkordi, M.E.; Luxami, V.; Pantoş, G.D. High-yielding synthesis of chiral donor—Acceptor catenanes. *J. Org. Chem.* **2018**, *83*, 11654–11660. [CrossRef] [PubMed]
14. Ponnuswamy, N.; Cougnon, F.B.L.; Pantoş, G.D.; Sanders, J.K.M. Homochiral and *meso* figure eight knots and a Solomon link. *J. Am. Chem. Soc.* **2014**, *136*, 8243–8251. [CrossRef]
15. Ponnuswamy, N.; Cougnon, F.B.L.; Clough, J.M.; Pantoş, G.D.; Sanders, J.K.M. Discovery of an organic trefoil knot. *Science* **2012**, *338*, 783–785. [CrossRef]
16. Stefankiewicz, A.R.; Sambrook, M.R.; Sanders, J.K.M. Template-directed synthesis of multi-component organic cages in water. *Chem. Sci.* **2012**, *3*, 2326. [CrossRef]
17. Stefankiewicz, A.R.; Sanders, J.K.M. Diverse topologies in dynamic combinatorial libraries from tri- and mono-thiols in water: Sensitivity to weak supramolecular interactions. *Chem. Commun.* **2013**, *49*, 5820. [CrossRef]
18. Furusho, Y.; Oku, T.; Hasegawa, T.; Tsuboi, A.; Kihara, N.; Takata, T. Dynamic covalent approach to [2]- and [3]Rotaxanes by Utilizing a reversible Thiol–Disulfide interchange reaction. *Chem.-Eur. J.* **2003**, *9*, 2895–2903. [CrossRef]
19. Kassem, S.; Lee, A.T.L.; Leigh, D.A.; Markevicius, A.; Solà, J. Pick-up, transport and release of a molecular cargo using a small-molecule robotic arm. *Nat. Chem.* **2015**, *8*, 138–143. [CrossRef]
20. Sun, J.; Patrick, B.O.; Sherman, J.C. A new [4]carceplex, and a crystal structure and dynamic combinatorial chemistry of a [5]carceplex. *Tetrahedron* **2009**, *65*, 7296–7302. [CrossRef]

21. Chichak, K.S.; Cantrill, S.J.; Pease, A.R.; Chiu, S.-H.; Cave, G.W.V.; Atwood, J.L.; Stoddart, J.F. Molecular borromean rings. *Science* **2004**, *304*, 1308–1312. [CrossRef]
22. Meyer, C.D.; Forgan, R.S.; Chichak, K.S.; Peters, A.J.; Tangchaivang, N.; Cave, G.W.V.; Khan, S.I.; Cantrill, S.J.; Stoddart, J.F. The dynamic chemistry of molecular borromean rings and solomon knots. *Chem.-Eur. J.* **2010**, *16*, 12570–12581. [CrossRef] [PubMed]
23. Pentecost, C.D.; Chichak, K.S.; Peters, A.J.; Cave, G.W.V.; Cantrill, S.J.; Stoddart, J.F. A molecular Solomon link. *Angew. Chem. Int. Ed.* **2007**, *46*, 218–222. [CrossRef]
24. Avestro, A.-J.; Gardner, D.M.; Vermeulen, N.A.; Wilson, E.A.; Schneebeli, S.T.; Whalley, A.C.; Belowich, M.E.; Carmieli, R.; Wasielewski, M.R.; Stoddart, J.F. Gated electron sharing within dynamic naphthalene Diimide-based Oligorotaxanes. *Angew. Chem. Int. Ed.* **2014**, *53*, 4442–4449. [CrossRef] [PubMed]
25. Belowich, M.E.; Valente, C.; Stoddart, J.F. Template-directed syntheses of rigid oligorotaxanes under thermodynamic control. *Angew. Chem. Int. Ed.* **2010**, *49*, 7208–7212. [CrossRef] [PubMed]
26. Bilbeisi, R.A.; Ronson, T.K.; Nitschke, J.R. A self-assembled [Fe $^{II}{}_{12}$ L $_{12}$] capsule with an icosahedral framework. *Angew. Chem. Int. Ed.* **2013**, *52*, 9027–9030. [CrossRef]
27. Black, S.P.; Stefankiewicz, A.R.; Smulders, M.M.J.; Sattler, D.; Schalley, C.A.; Nitschke, J.R.; Sanders, J.K.M. Generation of a Dynamic system of three-dimensional tetrahedral Polycatenanes. *Angew. Chem. Int. Ed.* **2013**, *52*, 5749–5752. [CrossRef]
28. Kieffer, M.; Pilgrim, B.S.; Ronson, T.K.; Roberts, D.A.; Aleksanyan, M.; Nitschke, J.R. Perfluorinated ligands induce Meridional metal stereochemistry to generate M_8L_{12}, $M_{10}L_{15}$, and $M_{12}L_{18}$ prisms. *J. Am. Chem. Soc.* **2016**, *138*, 6813–6821. [CrossRef]
29. Jansze, S.M.; Cecot, G.; Wise, M.D.; Zhurov, K.O.; Ronson, T.K.; Castilla, A.M.; Finelli, A.; Pattison, P.; Solari, E.; Scopelliti, R.; et al. Ligand aspect ratio as a decisive factor for the self-assembly of coordination cages. *J. Am. Chem. Soc.* **2016**, *138*, 2046–2054. [CrossRef]
30. Hasell, T.; Wu, X.; Jones, J.T.A.; Bacsa, J.; Steiner, A.; Mitra, T.; Trewin, A.; Adams, D.J.; Cooper, A.I. Triply interlocked covalent organic cages. *Nat. Chem.* **2010**, *2*, 750–755. [CrossRef]
31. Tozawa, T.; Jones, J.T.A.; Swamy, S.I.; Jiang, S.; Adams, D.J.; Shakespeare, S.; Clowes, R.; Bradshaw, D.; Hasell, T.; Chong, S.Y.; et al. Porous organic cages. *Nat. Mater.* **2009**, *8*, 973–978. [CrossRef]
32. Black, S.P.; Sanders, J.K.M.; Stefankiewicz, A.R. Disulfide exchange: Exposing supramolecular reactivity through dynamic covalent chemistry. *Chem. Soc. Rev.* **2014**, *43*, 1861–1872. [CrossRef] [PubMed]
33. Cougnon, F.B.L.; Sanders, J.K.M. Evolution of dynamic combinatorial chemistry. *Acc. Chem. Res.* **2012**, *45*, 2211–2221. [CrossRef]
34. Beeren, S.R.; Sanders, J.K.M. History and principles of dynamic combinatorial chemistry. In *Dynamic Combinatorial Chemistry*; Reek, J.N.H., Otto, S., Eds.; Wiley-VCH Verlag GmbH & Co. KGaA: Weinheim, Germany, 2010; pp. 1–22.
35. Christinat, N.; Scopelliti, R.; Severin, K. Boron-based rotaxanes by multicomponent self-assembly. *Chem. Commun.* **2008**, *31*, 3660–3662. [CrossRef] [PubMed]
36. Kataoka, K.; James, T.D.; Kubo, Y. Ion pair-driven Heterodimeric capsule based on Boronate esterification: Construction and the dynamic behavior. *J. Am. Chem. Soc.* **2007**, *129*, 15126–15127. [CrossRef]
37. Nishimura, N.; Kobayashi, K. Self-assembly of a cavitand-based capsule by dynamic boronic ester formation. *Angew. Chem. Int. Ed.* **2008**, *47*, 6255–6258. [CrossRef] [PubMed]
38. von Delius, M.; Geertsema, E.M.; Leigh, D.A. A synthetic small molecule that can walk down a track. *Nat. Chem.* **2010**, *2*, 96–101. [CrossRef] [PubMed]
39. von Delius, M.; Geertsema, E.M.; Leigh, D.A.; Tang, D.-T.D. Design, synthesis, and operation of small molecules that walk along tracks. *J. Am. Chem. Soc.* **2010**, *132*, 16134–16145. [CrossRef] [PubMed]
40. Pantoş, G.D.; Wietor, J.L.; Sanders, J.K.M. Filling helical nanotubes with C-60. *Angew. Chem. Int. Ed.* **2007**, *46*, 2238–2240. [CrossRef]
41. Pantoş, G.D.; Pengo, P.; Sanders, J.K.M. Hydrogen-bonded helical organic nanotubes. *Angew. Chem. Int. Ed.* **2007**, *46*, 194–197. [CrossRef]
42. Wietor, J.-L.; Pantoş, G.D.; Sanders, J.K.M. Templated amplification of an unexpected receptor for C70. *Angew. Chem. Int. Ed.* **2008**, *47*, 2689–2692. [CrossRef]
43. Cacciapaglia, R.; Di Stefano, S.; Ercolani, G.; Mandolini, L. Combinatorial macrocyclizations under thermodynamic control: The two-monomer case. *Macromolecules* **2009**, *42*, 4077–4083. [CrossRef]

44. Au-Yeung, H.Y.; Pantoş, G.D.; Sanders, J.K.M. Dynamic combinatorial donor−acceptor catenanes in water: Access to unconventional and unexpected structures. *J. Org. Chem.* **2011**, *76*, 1257–1268. [CrossRef]
45. Au-Yeung, H.Y.; Pantoş, G.D.; Sanders, J.K.M. Dynamic combinatorial synthesis of a catenane based on donor-acceptor interactions in water. *Proc. Natl. Acad. Sci. USA* **2009**, *106*, 10466–10470. [CrossRef]
46. Fass, D.; Thorpe, C. Chemistry and enzymology of disulfide cross-linking in proteins. *Chem. Rev.* **2018**, *118*, 1169–1198. [CrossRef]
47. Liu, T.; Wang, Y.; Luo, X.; Li, J.; Reed, S.A.; Xiao, H.; Young, T.S.; Schultz, P.G. Enhancing protein stability with extended disulfide bonds. *Proc. Natl. Acad. Sci. USA* **2016**, *113*, 5910–5915. [CrossRef]
48. Bosnjak, I.; Bojovic, V.; Segvic-Bubic, T.; Bielen, A. Occurrence of protein disulfide bonds in different domains of life: A comparison of proteins from the Protein Data Bank. *Protein Eng. Des. Sel.* **2014**, *27*, 65–72. [CrossRef] [PubMed]
49. Cougnon, F.B.L.; Ponnuswamy, N.; Jenkins, N.A.; Pantoş, G.D.; Sanders, J.K.M. Structural parameters Governing the dynamic combinatorial synthesis of catenanes in water. *J. Am. Chem. Soc.* **2012**, *134*, 19129–19135. [CrossRef] [PubMed]
50. Hanwell, M.D.; Curtis, D.E.; Lonie, D.C.; Vandermeersch, T.; Zurek, E.; Hutchison, G.R. Avogadro: An advanced semantic chemical editor, visualization, and analysis platform. *J. Cheminformatics* **2012**, *4*, 17. [CrossRef] [PubMed]
51. Stewart, J.J.P. Optimization of parameters for semiempirical methods VI: More modifications to the NDDO approximations and re-optimization of parameters. *J. Mol. Model.* **2013**, *19*, 1–32. [CrossRef] [PubMed]
52. Allouche, A.-R. Gabedit-A graphical user interface for computational chemistry softwares. *J. Comput. Chem.* **2011**, *32*, 174–182. [CrossRef] [PubMed]
53. Samsoniya, S.A.; Targamadze, N.L.; Suvorov, N.N. The chemistry of pyrroloindoles. *Russ. Chem. Rev.* **1994**, *63*, 815–832. [CrossRef]
54. Manjal, S.K.; Pathania, S.; Bhatia, R.; Kaur, R.; Kumar, K.; Rawal, R.K. Diversified synthetic strategies for pyrroloindoles: An overview. *J. Heterocycl. Chem.* **2019**, *56*, 2318–2332. [CrossRef]
55. Heaner, W.L., IV; Gelbaum, C.S.; Gelbaum, L.; Pollet, P.; Richman, K.W.; DuBay, W.; Butler, J.D.; Wells, G.; Liotta, C.L. Indoles via Knoevenagel–Hemetsberger reaction sequence. *RSC Adv.* **2013**, *3*, 13232–13242. [CrossRef]
56. Tan, Y.; Ghandi, K. Kinetics and mechanism of pyrrole chemical polymerization. *Synth. Met.* **2013**, *175*, 183–191. [CrossRef]
57. Donovalová, J.; Cigáň, M.; Stankovičová, H.; Gašpar, J.; Danko, M.; Gáplovský, A.; Hrdlovič, P. Spectral properties of substituted coumarins in solution and polymer matrices. *Molecules* **2012**, *17*, 3259–3276. [CrossRef]
58. Assaf, K.I.; Nau, W.M. The chaotropic effect as an assembly motif in chemistry. *Angew. Chem. Int. Ed.* **2018**, *57*, 13968–13981. [CrossRef]
59. Gianga, T.-M. Topologically Complex Molecules: Synthesis and Properties. PhD Thesis, University of Bath, Bath, UK, 2020.
60. Pengo, P.; Pantoş, G.D.; Otto, S.; Sanders, J.K.M. Efficient and mild microwave-assisted stepwise functionalization of Naphthalenediimide with α-amino acids. *J. Org. Chem.* **2006**, *71*, 7063–7066. [CrossRef]
61. Au-Yeung, H.Y.; Pengo, P.; Pantoş, G.D.; Otto, S.; Sanders, J.K.M. Templated amplification of a naphthalenediimide-based receptor from a donor–acceptor dynamic combinatorial library in water. *Chem. Commun.* **2009**, *4*, 419–421. [CrossRef]